J Eng Math (2008) 62:355–372
DOI 10.1007/s10665-008-9219-1

A boundary-integral method for the interaction of large-amplitude ocean waves with a compliant floating raft such as a sea-ice floe

Gareth M. Hegarty · Vernon A. Squire

Received: 8 July 2007 / Accepted: 12 February 2008 / Published online: 8 March 2008

Abstract The interaction of large-amplitude water waves with a compliant floating raft such as a sea-ice floe or a pontoon-type VLFS (very large floating structure) is considered. The solution is expressed as a series using a perturbation expansion, the first two components of which are solved inductively using a boundary-integral method. The primary interest of this paper is to the ways in which the second-order potential can be modified in order to apply the boundary-integral method and to the comparison of results with those derived using eigenfunction matching methods.

Keywords Boundary integral · Compliant raft · Large amplitude · Sea-ice · Waves

1 Introduction

Although (see [1]) there has been an abundance of theoretical papers focused upon flexural-gravity wave propagation in sea-ice [2–14], since the review article [15] there has been remarkably little work dealing with large-amplitude waves [16–18]. Yet, with the onset of global climate change and the attendant increase in extreme weather events, including storms, it is inevitable that high-energy ocean surface waves will occur more frequently and that these will drive further into the polar and subpolar seas, either as free-surface waves or as flexural-gravity waves travelling at the ice–water interface. Concomitantly, ice fields will be broken up more readily at greater penetrations than now—due to the higher waves but also to the weaker sea-ice arising on a warmer Earth, causing enhanced melting and a decrease in ice concentration. The greater number of polynyas and leads in the pack ice will potentially impact on regional climate because sea-ice affects the way the atmosphere couples to the ocean. Taken in the context of global warming, this is of immediate topical significance, first because temporal adjustments in pack ice serve as a proxy of climate change [19–21] but also because more open water will attract intensified oil and gas exploration and production accompanied by expanded offshore engineering, fabrication and management activities. Accordingly, there are compelling practical reasons for augmenting the linear studies cited above to include higher-amplitude waves but also to incorporate plate theories that properly take into account large-amplitude deflections.

G. M. Hegarty
School of Pharmacy, Division of Health Sciences, University of Otago, P.O. Box 56, Dunedin, New Zealand

V. A. Squire (✉)
Division of Sciences, University of Otago, P.O. Box 56, Dunedin, New Zealand
e-mail: vernon.squire@otago.ac.nz

In this context and in the manner of [22,23] we consider in this paper how an isolated flexible ice floe or raft of specified dimension responds to ocean waves—in this case of higher order. Notwithstanding that the immediate relevance of the work is to polar marine geophysics and, as a consequence, to offshore Arctic engineering and hydrocarbon extraction, this is only one possible application and for this reason we retain and signal generality by calling our floating body a compliant raft.

Discounting Jules Verne's idea of the seagoing 'Standard Island' introduced in his wonderful book L'île à Hélice [24], other applications that are each likely to be acted upon by significant seas include, for example, offshore port facilities that may incorporate provision for storage and waste disposal, energy islands including some wave-power configurations, flexible breakwaters, a supertanker in a seaway, or a pontoon-type hydroelastic VLFS (very large floating structure) such as a floating airport or a mobile offshore base. Such projects are associated with immense costs that are typically in the range US $5–$15B for design lives of 50–100 years. (Readers may already know of a 6-year plan launched in 1995 to research and develop Megafloat, a floating airport in Yokosuka Bay, Japan, which involved the construction of a 1,000 m by 60–121 m model that successfully passed takeoff and landing tests. A detailed evaluation of the tests on the 1,000 m Megafloat and the 4,000 m-class test design, concluded that a Megafloat airport with a scale of up to 4,000 m was more than feasible.)

The study herein has been a little more complicated and protracted than we first anticipated, as is explained in the text in relation to [16–18]. For example, it is shown that the so-called matching method conceived in [16] and used in [18] to describe surface waves incident upon a compliant floating raft such as a sea-ice floe in water of finite depth and which requires infinite series to be truncated, unexpectedly produces inaccurate results.

The paper begins by formulating the problem to be solved in mathematical terms and introducing the three types of plate equation that will be used; due to Forbes [25,26], von Kármán (see [27, Sect. 16.9] and [28, Sect. 8.5]) and Drozdov [29, pp. 191–196]. The solution method is then introduced, including both first- and second-order formulations. The authors have also spent time validating their results by means of two classes of potential, a Neumann-type (Appendix B.1) and a wave-type (Appendix B.2). Finally, to finish, some examples are given that compare first- and second-order predictions, so that their relative importance can be established under different ocean-wave forcing scenarios.

2 Formulation

We consider a long-crested travelling wave of amplitude a propagating at the surface of water of infinite depth and density ρ_w, incident on a compliant floating raft of length L, density ρ_i and thickness h. We assume that the fluid is incompressible and irrotational. A velocity potential Φ may then be defined that satisfies Laplace's equation

$$\Delta\Phi = 0, \tag{1}$$

where the operator $\Delta = \nabla^2 = \partial^2/\partial x^2 + \partial^2/\partial z^2$ and the sea-floor condition

$$\Phi_z = 0, \quad z \to \infty. \tag{2}$$

In two of the plate models considered for the floe [29, pp. 191–196] and [25,26] the sea surface is given everywhere as $z = -\eta(x,t)$, which satisfies the Bernoulli-pressure surface condition

$$-\frac{mg}{\rho_w} + g\eta + \Phi_t + \frac{1}{2}\left((\Phi_x)^2 + (\Phi_z)^2\right) + \frac{p}{\rho_w} = 0, \quad z = -\eta, \tag{3}$$

where $m = \rho_i h$ is the mass per unit area, g is the acceleration due to gravity, and the kinematic surface condition

$$\Phi_x\eta_x + \eta_t + \Phi_z = 0, \quad z = -\eta, \tag{4}$$

as derived in [30, p. 16]. For the von Kármán plate [27, Sect. 16.9], [28, Sect. 8.5], the surface is given as $(x+u(x,t), -\eta(x,t))$ for $x \in [0, L]$. In this case the Bernoulli equation (3) looks exactly the same but is applied at $(x+u, -\eta)$, while the kinematic equation becomes

$$\eta_t + \frac{\eta_x}{1+u_x}\Phi_x(x+u, -\eta(x,t)) + \Phi_z(x+u, -\eta(x,t)) = 0. \tag{5}$$

The pressure term $p(x,t)$ in the Bernoulli equation is derived from the plate equation for the force exerted upon the surface. The approach used is 'direct' in the sense that a single set of equations for Φ will be solved, as opposed to treating the hydrodynamics and material deformation separately. Denoting the flexural rigidity by $D = Eh^3/12(1-\nu^2)$, where E is Young's modulus and ν is Poisson's ratio, we consider three different nonlinear models for the plate due to Forbes [25,26], von Kármán [27, Sect. 16.9], [28, Sect. 8.5] and Drozdov [29, pp. 191–196]. In each case the model is an extension to the standard Kirchhoff (Euler–Bernoulli) plate formulation, which incorporates different geometrically nonlinear terms. More general nonlinear models are possible, of course, but these would introduce significantly more complicated algebra. (For example, one might reasonably allow the ends of the plates to move laterally to assimilate the effect of floe drift.) The plate models used herein are described mathematically in Sects. 2.1–2.3.

2.1 Forbes

$$p = M_{xx} + m(\eta_{tt} + g), \quad 0 < x < L, \tag{6}$$

where

$$M = \frac{2D\eta_{xx}}{(2+\eta_x^2)^{3/2} - h\eta_{xx}}.$$

Rather than using the linearized approximate version of curvature that appears in the Euler–Bernoulli plate equation, this plate equation incorporates the Gaussian curvature in full. Axial forces are not included, however.

2.2 von Kármán

The basic assumption of the von Kármán plate is that, although the deflexion is no longer small in comparison with the plate thickness, it still remains small in comparison with the plate's lateral dimensions. As noted above, the surface in this case is given as $(x + u(x,t), -\eta(x,t))$ and the pressure is given by

$$p = M_{xx} - N\eta_{xx} + m(\eta_{tt} + g), \tag{7}$$

where

$$M = D\eta_{xx},$$

and

$$N = \frac{Eh}{(1-\nu^2)}\left(u_x + \frac{1}{2}\eta_x^2\right) = \frac{Eh}{2(1-\nu^2)L}\int_0^L \eta_x^2 \mathrm{d}x,$$

is the resultant axial stress. This can be written in the latter form, which is independent of $u(x,t)$, because $\partial N/\partial x = 0$ and we have assumed $u(0,t) = u(L,t) = 0$.

2.3 Drozdov

In this model the vertical force on the plate is

$$p\cos\alpha = \frac{\partial}{\partial x}(M_x - N\eta_x) + m(\eta_{tt} + g), \tag{8}$$

where

$$M = \frac{2D\eta_{xx}}{2(1+\eta_x^2)^{3/2} - h\eta_{xx}}, \quad N = Eh\left((1+\eta_x^2)^{1/2} - 1\right),$$

and $\alpha(x,t)$ is the angle the curve $z = -\eta(x,t)$ makes with the vertical. The Drozdov plate equation is a more general version of the Forbes one in the sense that Gaussian curvature is used but, analogous to the von Kármán theory, the formulation includes axial stresses N (although in this case $\partial N/\partial x \neq 0$) and the provision for the pressure to always act normally to the deforming surface at the underside of the raft.

2.4 Nondimensionalization

In each case the problem is nondimensionalized by multiplying all lengths by the travelling wave number $\sigma_0 = \omega^2/g$ and times by the quantity $\sqrt{\sigma_0 g}$. Consequently, the potential, bending moment, resultant axial stress and pressure are, respectively, scaled as follows:

$$\overline{\Phi} = \sqrt{\sigma_0^3/g}\,\Phi, \quad \overline{M} = \sigma_0^3 M/\rho_i g, \quad \overline{N} = \frac{\sigma_0}{\rho_i g} N, \quad \overline{p} = \frac{\sigma_0}{\rho_w g} p.$$

Henceforth, omitting the overbars, the nondimensional governing equations are given by

$$\Delta\Phi = 0, \tag{9a}$$

$$\Phi_z = 0, \quad z \to \infty, \tag{9b}$$

$$\eta + \Phi_t + (\Phi_x^2 + \Phi_z^2) + p - \gamma = 0, \quad z = -\eta, \tag{9c}$$

$$\eta_t + \Phi_z + \Phi_x \eta_x = 0, \quad z = -\eta, \tag{9d}$$

for the Forbes and Drozdov plate models, where $\gamma = \sigma_0 h \rho_i/\rho_w$. For the von Kármán plate the nondimensional Bernoulli equation appears exactly the same as above but is evaluated at $(x + u, -\eta)$, while the nondimensional form of the kinematic condition (5) is also the same. Finally, we nondimensionalize the plate models (6)–(8), scaling each by $\sigma_0/\rho_w g$. So, in the case of the Forbes model, for example, we have

$$M_{xx} + \gamma \eta_{tt} + \gamma = p, \quad 0 < x < L, \tag{10}$$

where

$$M = \frac{\beta \eta_{xx}}{(1+\eta_x^2)^{3/2} - h\eta_{xx}/2}, \quad \beta = \frac{D\sigma_0^4}{\rho_w g}.$$

We also apply free-edge conditions at each end of the plate, i.e.,

$$M = M_x = 0 \quad \text{at } x \in \{0^+, L^-\}. \tag{11}$$

3 Perturbation expansion

We use a Stokes expansion to investigate nonlinear effects. Recalling that a is the incident wave amplitude, we expand the potential, displacement and pressure as

$$\Phi(x,z,t) = \epsilon\Phi^{(1)}(x,z,t) + \epsilon^2\Phi^{(2)}(x,z,t) + \cdots \tag{12a}$$

$$\eta(x,t) = \epsilon\eta^{(1)}(x,t) + \epsilon^2\eta^{(2)}(x,t) + \cdots \tag{12b}$$

$$p(x,t) = p^{(0)}(x,t) + \epsilon p^{(1)}(x,t) + \epsilon^2 p^{(2)}(x,t) + \cdots \tag{12c}$$

where $\epsilon = a\sigma_0$ is a small parameter and, for the von Kármán plate, we expand the horizontal displacement

$$u(x,t) = \epsilon^2 u^{(2)}(x,t) + \epsilon^3 u^{(3)}(x,t) + \cdots. \tag{13}$$

We then use a Taylor series to expand the potential on the surface (and its derivatives) about the mean surface $z = 0$

$$\begin{aligned}\Phi(x,\eta,t) &= \Phi(x,0,t) - \eta\Phi_z(x,0,t) + \frac{\eta^2}{2}\Phi_{zz}(x,0,t) + \cdots \\ &= \epsilon\Phi^{(1)}(x,0,t) + \epsilon^2\left(\Phi^{(2)}(x,0,t) - \Phi_z^{(1)}(x,0,t)\eta^{(1)}(x,t)\right) + \cdots\end{aligned} \tag{14}$$

Substituting $\Phi(x,\eta,t)$ and $\eta(x,t)$ in the Bernoulli surface pressure condition and separating orders of ϵ gives the system of equations

$$p^{(1)} + \Phi_t^{(1)} + \eta^{(1)} = 0, \tag{15a}$$

$$\frac{1}{2}\left((\Phi_x^{(1)})^2 + (\Phi_z^{(1)})^2\right) - \Phi_{zt}^{(1)}\eta^{(1)} + p^{(2)} + \Phi_t^{(2)} + \eta^{(2)} = 0, \tag{15b}$$

$$\vdots$$

Similarly, substituting $\Phi(x,\eta,t)$ and $\eta(x,t)$ in the kinematic surface condition gives

$$\eta_t^{(1)} + \Phi_z^{(1)} = 0, \tag{16a}$$

$$\Phi_x^{(1)}\eta_x^{(1)} - \Phi_{zz}^{(1)}\eta^{(1)} + \eta_t^{(2)} + \Phi_z^{(2)} = 0, \tag{16b}$$

$$\vdots$$

Observe that the second-order Bernoulli and kinematic equations are exactly the same for each of the plate models. Substituting $\eta(x,t)$ in the plate equation gives the system

$$\beta\eta_{xxxx}^{(1)} + \gamma\eta_{tt}^{(1)} = p^{(1)}, \tag{17a}$$

$$\beta\eta_{xxxx}^{(2)} + \gamma\eta_{tt}^{(2)} + \beta h(\eta_{xx}^{(1)^2})_{xx}/2 = p^{(2)}, \tag{17b}$$

$$\vdots$$

Finally, the edge conditions give

$$\eta_{xx}^{(1)} = \eta_{xxx}^{(1)} = 0, \ x = 0, \ L, \tag{18a}$$

$$\eta_{xx}^{(2)} = \eta_{xxx}^{(2)} = 0, \ x = 0, \ L, \tag{18b}$$

$$\vdots$$

4 First order solution

We begin by assuming that the first-order velocity potential can be written as $\Phi^{(1)}(x,z,t) = \phi^{(1)}(x,z)\mathrm{e}^{\mathrm{i}t}$. The first-order solution to the problem arises from solving the first-order parts of the perturbation expansion for $\phi^{(1)}(x,z)$, i.e.,

$$\Delta\phi^{(1)} = 0, \quad z > 0, \tag{19a}$$

$$\phi_z^{(1)} + \phi^{(1)} = 0, \quad z = 0, \quad x < 0 \quad \text{or} \quad x > L, \tag{19b}$$

$$\beta\phi_{zxxxx}^{(1)} + (1-\gamma)\phi_z^{(1)} + \phi^{(1)} = 0, \quad z = 0, \quad 0 < x < L, \tag{19c}$$

$$\phi_{zxx}^{(1)} = \phi_{zxxx}^{(1)} = 0, \quad z = 0, \quad x = 0 \quad \text{or} \quad x = L, \tag{19d}$$

$$\phi^{(1)} \to \mathrm{e}^{-\mathrm{i}x} + R^{(1)}\mathrm{e}^{\mathrm{i}x}, \quad x \to -\infty, \tag{19e}$$

$$\phi^{(1)} \to T^{(1)}\mathrm{e}^{-\mathrm{i}x}, \quad x \to \infty. \tag{19f}$$

where $R^{(1)}$ and $T^{(1)}$ are the first-order reflection and transmission coefficients, respectively. Since $\phi^{(1)}(x,z)$ satisfies Laplace's equation in the half-plane $z > 0$, we may invoke Green's theorem in the plane

$$\phi^{(1)}(x,z) = \int_\Gamma \phi^{(1)}G_n^{(1)} - \phi_n^{(1)}G^{(1)}\mathrm{d}s, \tag{20}$$

where Γ is a contour including (x,z) extending from $\xi = -\infty$ to ∞ and from $\zeta = 0$ to ∞, as in Fig. 1, and $G^{(1)}(\xi,\zeta;x,z)$ is the well-known first-order open-water infinite-depth Green's function given by

$$G^{(1)}(\xi,\zeta;x,z) = -\frac{1}{2\pi}\int_{-\infty}^{\infty}\frac{\mathrm{e}^{-|k|(z+\zeta)+\mathrm{i}k(\xi-x)}}{|k|-1}\mathrm{d}k + \frac{1}{4\pi}\log\left((x-\xi)^2+(z-\zeta)^2\right) - \frac{1}{4\pi}\log\left((x-\xi)^2+(z+\zeta)^2\right). \tag{21}$$

Using the asymptotic expressions for $\phi^{(1)}$ and $G^{(1)}$ and the boundary conditions, we may write integral equation (20) on the surface $z = 0$ as

$$\phi^{(1)}(x,0) = \mathrm{e}^{-\mathrm{i}x} + \int_0^L \tilde{G}(\xi,x)\psi(\xi)\mathrm{d}\xi, \tag{22a}$$

$$\psi(\xi) = \phi^{(1)}(\xi,0) + \phi_\zeta^{(1)}(\xi,0), \tag{22b}$$

where $\tilde{G}(\xi,x) = G^{(1)}(\xi,0;x,0) + \mathrm{i}\cos(\xi - x)$.

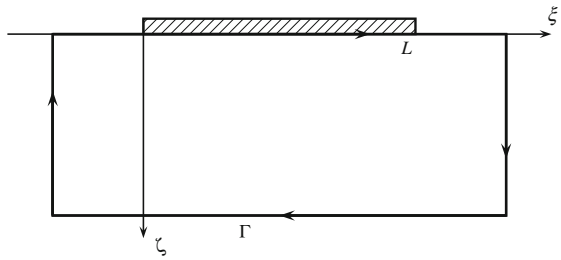

Fig. 1 The contour of integration used in the application of Green's theorem (20). The hatched area represents the compliant raft

Next we use a second (dry) Green's function for the plate alone to write $\phi_z^{(1)}$ in terms of $\phi^{(1)}$ under the raft, i.e.,

$$\phi_z^{(1)}(x,0) = -\frac{1}{\beta}\int_0^L \bar{g}^{(1)}(\xi,x)\phi^{(1)}(\xi,0)\mathrm{d}\xi, \quad 0 \le x \le L. \tag{23}$$

where $\bar{g}^{(1)}(\xi,x)$ is the dry Green's function for the plate, satisfying

$$\frac{\mathrm{d}^4\bar{g}^{(1)}(\xi,x)}{\mathrm{d}\xi^4} - \mu_1^4 g^{(1)}(\xi,x) = \delta(\xi - x), \tag{24}$$

where $\mu_1 = \sqrt[4]{(\gamma-1)/\beta}$ and the free-edge boundary conditions

$$\bar{g}^{(1)}_{\xi\xi}(0,x) = \bar{g}^{(1)}_{\xi\xi}(L,x) = \bar{g}^{(1)}_{\xi\xi\xi}(0,x) = \bar{g}^{(1)}_{\xi\xi\xi}(L,x) = 0. \tag{25}$$

The Green's function $\bar{g}^{(1)}(\xi,x)$ is given piecewise as

$$\frac{1}{\beta}\bar{g}^{(1)}(\xi,x) = \begin{cases} A_1\mathrm{e}^{\mathrm{i}\mu_1\xi} + B_1\mathrm{e}^{-\mathrm{i}\mu_1\xi} + C_1\mathrm{e}^{\mu_1\xi} + D_1\mathrm{e}^{-\mu_1\xi}, & 0 < \xi < x < L, \\ A_2\mathrm{e}^{\mathrm{i}\mu_1\xi} + B_2\mathrm{e}^{-\mathrm{i}\mu_1\xi} + C_2\mathrm{e}^{\mu_1\xi} + D_2\mathrm{e}^{-\mu_1\xi}, & 0 < x < \xi < L, \end{cases} \tag{26}$$

where

$$\begin{pmatrix} A_1 \\ B_1 \\ C_1 \\ D_1 \end{pmatrix} = -\frac{1}{2\beta\mu_1^3}\begin{pmatrix} -1 & -1 & 1 & 1 \\ -\mathrm{i} & \mathrm{i} & 1 & -1 \\ -\mathrm{e}^{\mathrm{i}\mu_1 L} & -\mathrm{e}^{-\mathrm{i}\mu_1 L} & \mathrm{e}^{\mu_1 L} & \mathrm{e}^{-\mu_1 L} \\ -\mathrm{i}\mathrm{e}^{\mathrm{i}\mu_1 L} & \mathrm{i}\mathrm{e}^{-\mathrm{i}\mu_1 L} & \mathrm{e}^{\mu_1 L} & -\mathrm{e}^{-\mu_1 L} \end{pmatrix}^{-1} \times \begin{pmatrix} 0 \\ 0 \\ \sin\mu_1(L-x) + \sinh\mu_1(L-x) \\ \cos\mu_1(L-x) + \cosh\mu_1(L-x) \end{pmatrix},$$

and

$$\begin{pmatrix} A_2 \\ B_2 \\ C_2 \\ D_2 \end{pmatrix} = \begin{pmatrix} A_1 \\ B_1 \\ C_1 \\ D_1 \end{pmatrix} + \frac{1}{4\beta\mu_1^3}\begin{pmatrix} \mathrm{i}\mathrm{e}^{-\mathrm{i}\mu_1 x} \\ -\mathrm{i}\mathrm{e}^{\mathrm{i}\mu_1 x} \\ \mathrm{e}^{-\mu_1 x} \\ \mathrm{e}^{\mu_1 x} \end{pmatrix}.$$

Finally, Eq. (23) is substituted back in the integral equation (22) to get

$$\phi^{(1)}(x,0) = \mathrm{e}^{-\mathrm{i}x} + \int_0^L \tilde{G}(\xi,x) \times \left(\phi^{(1)}(\xi,0) - \frac{1}{\beta}\int_0^L \bar{g}^{(1)}(\xi,\lambda)\phi^{(1)}(\lambda,0)\mathrm{d}\lambda\right)\mathrm{d}\xi. \tag{27}$$

Equation (27) is solved discretely for $\phi^{(1)}$ under the floe. We use a constant-element BEM to do this, dividing the interval $[0, L]$ into N evenly spaced subintervals and assuming that $\phi^{(1)}(x,0)$ is constant on each one, i.e.,

$$\phi^{(1)}(x,0) = \phi_j^{(1)}, \quad s_{j-1} < x < s_j, \quad j = 1,\ldots,N. \tag{28}$$

Under this assumption (27) becomes a linear system of N unknowns $\phi_j^{(1)}$ that is easily solved. Discrete values for the normal derivative $\phi_z^{(1)}(x,0)$ under the floe can then be found by discretizing (23), i.e.,

$$\phi_z^{(1)}(x,0) = \phi_{z_j}^{(1)}, \quad s_{j-1} < x < s_j, \quad j = 1,\ldots,N. \tag{29}$$

Once we have these, we can apply (22) again to get a smoother representation of $\phi^{(1)}(x,0)$, both inside and outside of the floe, i.e.,

$$\phi^{(1)}(x,0) = \mathrm{e}^{-\mathrm{i}x} + \sum_{j=1}^{N}\psi_j\int_{s_{j-1}}^{s_j}\tilde{G}\mathrm{d}\xi, \quad \psi_j = \phi_j^{(1)} + \phi_{z_j}^{(1)}. \tag{30a,b}$$

5 Second-order solution

We begin by assuming that the second-order velocity potential can be written as $\Phi^{(2)}(x,z,t)=\phi^{(2)}(x,z)\mathrm{e}^{2\mathrm{i}t}$. We then derive equations for $\phi^{(2)}$ from the second-order equations in the perturbation expansion, i.e.,

$$\Delta\phi^{(2)} = 0, \quad z>0, \tag{31a}$$

$$\phi_z^{(2)}+4\phi^{(2)} = 2\mathrm{i}A-B, \quad z=0, \quad x<0, \quad x>L, \tag{31b}$$

$$\beta(\phi_z^{(2)}+B)_{xxxx}+(1-4\gamma)(\phi_z^{(2)}+B)+4\phi^{(2)} = 2\mathrm{i}(A+C), \quad z=0, \quad 0<x<L, \tag{31c}$$

$$(\phi_z^{(2)}+B)_{xx}=(\phi_z^{(2)}+B)_{xxx} = 0, \quad z=0, \quad x=0 \quad \text{or} \quad x=L, \tag{31d}$$

$$\phi^{(2)}(x,0)\to 2\mathrm{i}R^{(1)}+R^{(2)}\mathrm{e}^{4\mathrm{i}x}, \quad \text{as } x\to-\infty, \tag{31e}$$

$$\phi^{(2)}(x,0)\to T^{(2)}\mathrm{e}^{-4\mathrm{i}x}, \quad \text{as } x\to\infty, \tag{31f}$$

where

$$A(x)=\frac{(\phi_x^{(1)})^2+(\phi_z^{(1)})^2}{2}-\mathrm{i}\eta^{(1)}\phi_z^{(1)}, \quad B(x)=\eta_x^{(1)}\phi_x^{(1)}-\eta^{(1)}\phi_{zz}^{(1)},$$

and

$$C(x)=0 \quad \text{(von Kármán)},$$

$$\text{or } C(x)=\frac{\beta h}{2}\left[\eta_x^{(1)}\right]_{xx}^2 \quad \text{(Forbes)},$$

$$\text{or } C(x)=\frac{\beta h}{2}\left[\eta_x^{(1)}\right]_{xx}^2+\gamma\left[\eta_x^{(1)}\right]^2 \quad \text{(Drozdov)}.$$

The first thing to notice about the second-order equations is that the equation under the floe is just a plate equation for $\phi_z^{(2)}+B$. Accordingly, we can write

$$\phi_z^{(2)}+B=\frac{1}{\beta}\int_0^L \bar{g}^{(2)}(x,\xi)\left(-4\phi^{(2)}(\xi,0)+2\mathrm{i}\left(A(\xi)+C(\xi)\right)\right)\mathrm{d}\xi. \tag{32}$$

where $\bar{g}^{(2)}(x,\xi)$ is the second-order dry Green's function for the plate satisfying equations similar to (24)–(25), but with $\mu_2=\sqrt[4]{(4\gamma-1)/\beta}$ in place of μ_1. In order to apply the boundary-integral method we make several modifications to $\phi^{(2)}$. Specifically, we consider instead

$$\varphi^{(2)}=\phi^{(2)}-\mathrm{i}R^{(1)}+q. \tag{33}$$

5.1 Using the Neumann-type singular potential

The Neumann-type singular solution (73) may now be employed in (33) to construct the system

$$\Delta\varphi^{(2)} = 0, \quad z>0, \tag{34a}$$

$$\varphi_z^{(2)}+4\varphi^{(2)} = -K_2-4\mathrm{i}R^{(1)}+4q, \quad z=0, \quad x<0, \quad x>L, \tag{34b}$$

$$\varphi_z^{(2)} = -K_2-2\mathrm{i}A+\frac{1}{\beta}\int_0^L \bar{g}^{(2)}(x,\xi)\left(-4\varphi^{(2)}(\xi,0)-4\mathrm{i}R^{(1)}\right.$$
$$\left.+4q(\xi,0)+2\mathrm{i}\left(A(\xi)+C(\xi)\right)\right)\mathrm{d}\xi, \quad z=0, \quad 0<x<L, \tag{34c}$$

$$\varphi^{(2)}(x,z)\to \mathrm{i}R^{(1)}+R^{(2)}\mathrm{e}^{4\mathrm{i}x-4z}, \quad x\to-\infty, \tag{34d}$$

$$\varphi^{(2)}(x,z)\to -\mathrm{i}R^{(1)}+T^{(2)}\mathrm{e}^{-4\mathrm{i}x-4z}, \quad x\to\infty. \tag{34e}$$

Applying Green's theorem to $\varphi^{(2)}$ as in Fig. 1, we derive the integral equation

$$\varphi^{(2)}(x,z) = \frac{R^{(2)}}{2}\mathrm{e}^{4\mathrm{i}x-4z} + \frac{T^{(2)}}{2}\mathrm{e}^{-4\mathrm{i}x-4z} - \int_{-\infty}^{0} G^{(2)}(K_2(\xi) + 4\mathrm{i}R^{(1)} - 4q(\xi,0))\mathrm{d}\xi$$
$$- \int_{L}^{\infty} G^{(2)}(K_2(\xi) + 4\mathrm{i}R^{(1)} - 4q(\xi,0))\mathrm{d}\xi + \int_0^L G^{(2)}\left(4\varphi^{(2)}(\xi,0) - K_2(\xi) - 2\mathrm{i}A(\xi)\right.$$
$$\left. + \frac{1}{\beta}\int_0^L \bar{g}^{(2)}(\xi,\lambda)\left(-4\varphi^{(2)}(\lambda,0) - 4\mathrm{i}R^{(1)} + 4q(\lambda,0) + 2\mathrm{i}\left(A(\lambda)+C(\lambda)\right)\right)\mathrm{d}\lambda\right)\mathrm{d}\xi, \tag{35}$$

where $G^{(2)}(\xi,\zeta;x,z)$ is the second-order open-water Green's function satisfying

$$\begin{aligned}\Delta G^{(2)} &= \delta(\xi-x,\zeta-z)\\ G^{(2)}_{\zeta} + 4G^{(2)} &= 0, \quad \zeta = 0\\ G^{(2)}_{\zeta} &\to 0, \quad \zeta\to\infty.\end{aligned}$$

Then, by invoking the symmetry of $G^{(2)}$ and applying the asymptotic conditions on φ as $x\to\pm\infty$ to provide expressions for $R^{(2)}$ and $T^{(2)}$, we may rewrite (35) and use (33) to obtain the following expression for $\phi^{(2)}$

$$\phi^{(2)}(x,z) = \mathrm{i}R^{(1)} - q(x,z) + 2R^{(1)}\mathrm{e}^{-4z}\sin 4x - \int_{-\infty}^{\infty}\tilde{G}^{(2)}\left(K_2(\xi) + 4\mathrm{i}R^{(1)} - 4\mathrm{i}R^{(1)}\mathrm{sgn}(\xi)\right)\mathrm{d}\xi$$
$$+4\int_{-\infty}^{\infty}\tilde{G}^{(2)}q(\xi,0)\mathrm{d}\xi - 8\mathrm{i}R^{(1)}\int_0^x G^{(2)}\mathrm{d}\xi + \int_0^L \tilde{G}^{(2)}\left(4\phi^{(2)}(\xi,0) - 2\mathrm{i}A(\xi)\right.$$
$$\left. + \frac{1}{\beta}\int_0^L \bar{g}^{(2)}(\xi,\lambda)\left(-4\phi^{(2)}(\lambda,0) + 2\mathrm{i}\left(A(\lambda)+C(\lambda)\right)\right)\mathrm{d}\lambda\right)\mathrm{d}\xi, \tag{36}$$

where $\tilde{G}^{(2)} = G^{(2)}(\xi,0;x,z) + \mathrm{i}\mathrm{e}^{-4z}\cos 4(\xi-x)$. Equation (36) can be solved numerically for $\phi^{(2)}(x,0)$ within $0<x<L$, which then allows us to evaluate $\phi^{(2)}(x,z)$ anywhere in the domain from the same equation.

5.2 Using the wave-type singular potential

If instead of Appendix B.1 we use the singular wave-type potential from Appendix B.2 then, combining the equations for $\phi^{(2)}$ and q, we obtain the system

$$\Delta\varphi^{(2)} = 0, \quad z>0, \tag{37a}$$
$$\varphi^{(2)}_z + 4\varphi^{(2)} = -K_2 - 4\mathrm{i}R^{(1)}, \quad z=0, \quad x<0, \quad x>L, \tag{37b}$$
$$\varphi^{(2)}_z = -K_2 - 2\mathrm{i}A - 4q + \frac{1}{\beta}\int_0^L \bar{g}^{(2)}(x,\xi)$$
$$\times\left(-4\varphi^{(2)}(\xi,0) - 4\mathrm{i}R^{(1)} + 4q(\xi,0) + 2\mathrm{i}\left(A(\xi)+C(\xi)\right)\right)\mathrm{d}\xi, \quad z=0, \quad 0<x<L, \tag{37c}$$
$$\varphi^{(2)}(x,z) \to \mathrm{i}R^{(1)} + \left(\left(R^{(2)} - \frac{\alpha_1}{2}\right)\mathrm{e}^{4\mathrm{i}x} - \frac{\alpha_2}{2}\mathrm{e}^{-4\mathrm{i}x}\right)\mathrm{e}^{-4z}, \quad x\to-\infty, \tag{37d}$$
$$\varphi^{(2)}(x,z) \to -\mathrm{i}R^{(1)} + \left(\frac{\alpha_1}{2}\mathrm{e}^{4\mathrm{i}x} + \left(T^{(2)} + \frac{\alpha_2}{2}\right)\mathrm{e}^{-4\mathrm{i}x}\right)\mathrm{e}^{-4z}, \quad x\to\infty, \tag{37e}$$

and, as for Sect. 5.1,

$$\varphi^{(2)}(x,z) = \frac{R^{(2)}}{2}\mathrm{e}^{4\mathrm{i}x-4z} + \frac{T^{(2)}}{2}\mathrm{e}^{-4\mathrm{i}x-4z} - \int_{-\infty}^{0} G^{(2)}\left(K_2(\xi) + 4\mathrm{i}R^{(1)}\right)\mathrm{d}\xi$$
$$- \int_{L}^{\infty} G^{(2)}(K_2(\xi) + 4\mathrm{i}R^{(1)})\mathrm{d}\xi + \int_0^L G^{(2)}\left(4\varphi^{(2)}(\xi,0) - K_2(\xi) - 2\mathrm{i}A(\xi) - 4q(\xi,0)\right.$$
$$\left. + \frac{1}{\beta}\int_0^L \bar{g}^{(2)}(\xi,\lambda)\left(-4\varphi^{(2)}(\lambda,0) - 4\mathrm{i}R^{(1)} + 4q(\lambda,0) + 2\mathrm{i}\left(A(\lambda)+C(\lambda)\right)\right)\mathrm{d}\lambda\right)\mathrm{d}\xi. \tag{38}$$

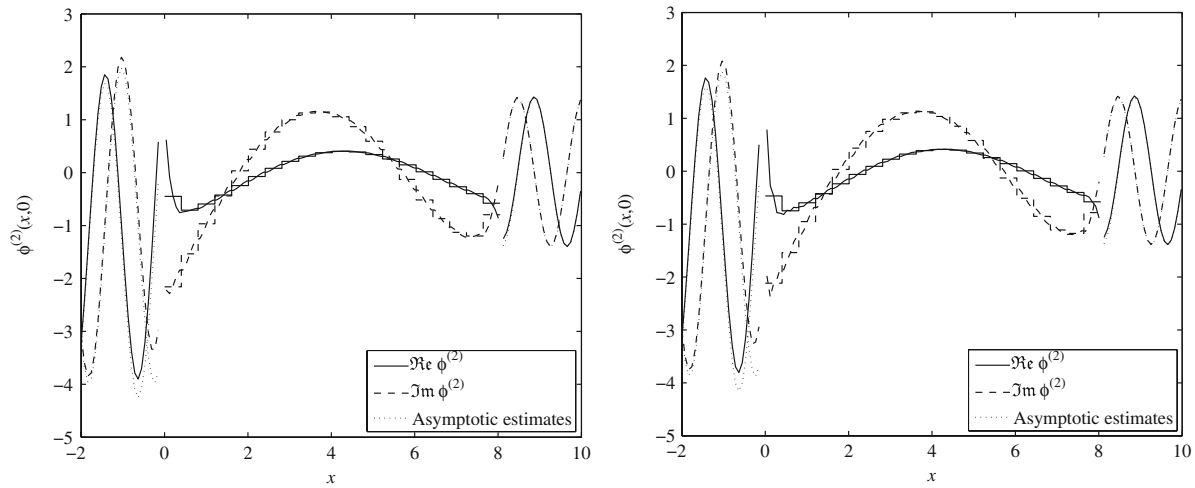

Fig. 2 Second-order potential $\phi^{(2)}(x,0)$ calculated using a Neumann-type (left plot) singular potential and a wave-type singular potential (right plot) for a 50 m by 1 m compliant raft in 1 m amplitude waves of period 5 s

We may then apply the asymptotic conditions to get formulae for $R^{(2)}$ and $T^{(2)}$ to obtain

$$\begin{aligned}\phi^{(2)}(x,z) = {} & \mathrm{i}R^{(1)} - q(x,z) + \left(2R^{(1)}\sin 4x + \frac{\alpha_1}{2}\mathrm{e}^{4\mathrm{i}x} - \frac{\alpha_2}{2}\mathrm{e}^{-4\mathrm{i}x}\right)\mathrm{e}^{-4z} \\ & - \int_{-\infty}^{\infty}\tilde{G}^{(2)}\left(K_2(\xi) + 4\mathrm{i}R^{(1)} - 4\mathrm{i}R^{(1)}\mathrm{sgn}(\xi)\right)\mathrm{d}\xi - 8\mathrm{i}R^{(1)}\int_0^x G^{(2)}\mathrm{d}\xi \\ & + \int_0^L \tilde{G}^{(2)}\left(4\phi^{(2)}(\xi,0) - 2\mathrm{i}A(\xi) + \frac{1}{\beta}\int_0^L \bar{g}^{(2)}(\xi,\lambda)\left(-4\phi^{(2)}(\lambda,0) + 2\mathrm{i}\left(A(\lambda)+C(\lambda)\right)\right)\mathrm{d}\lambda\right)\mathrm{d}\xi.\end{aligned} \tag{39}$$

where α_1 and α_2 are given in (79) and (80), respectively. Recall that one can easily recover the surface conditions from either (36) or (39) using

$$G_z^{(2)}(\xi,0;x,0) + 4G^{(2)}(\xi,0;x,0) = \delta(\xi - x). \tag{40}$$

Also note that the integral equations for $\phi^{(2)}$ in (36) and (39) are actually identical since

$$q^w - q^n + 4\int_{-\infty}^{\infty}\tilde{G}^{(2)}q^n(\xi,0)\mathrm{d}\xi = \frac{\alpha_1}{2}\mathrm{e}^{4\mathrm{i}x-4z} - \frac{\alpha_2}{2}\mathrm{e}^{-4\mathrm{i}x-4z}, \tag{41}$$

where q^n and q^w denote the Neumann-type and wave-type singular potentials, respectively. The second-order potentials arising from the two different approaches are shown in Fig. 2, where it can be seen that the two methods produce identical results.

6 Wave-type singular potential in finite depth

Here we investigate the applicability of the *matching method* to problems similar to those above but in water of finite depth. To simplify the discussion we focus on a wave-type potential problem in finite water depth similar to that in Sect. 6.2. We solve this problem by two methods, viz. residues and matching, and find that the matching method fails due to its inability to account for the singular behaviour at the origin properly.

Consider the equations for the wave-type singular potential in water of (nondimensional) depth H, i.e.,

$$\Delta q = 0, \quad z > 0, \tag{42a}$$

$$q_z + 4\omega^2 q = f(x), \quad z = 0, \tag{42b}$$

$$q_z = 0, \quad z = H, \tag{42c}$$

where ω is the nondimensional frequency. In common with our earlier discussion, we choose $f(x) = \mathrm{e}^{x}U(-x)/x$ and use the same nondimensionalization as [16]. Taking the Fourier transform, we may derive the solution

$$q(x,z) = -\frac{1}{2\pi}\int_{-\infty}^{\infty} \frac{\hat{f}(k)}{k\tanh kH - 4\omega^2}\,\chi(k,z)\,\mathrm{e}^{-\mathrm{i}kx}\mathrm{d}k, \tag{43}$$

where $\chi(k,z) = \cosh k(z-H)/\cosh kH$. Next, note how the Green's function for open water of infinite depth is approximated by the series expression for the Green's function using an expression derived in [31]. From the series representation of the Green's function for open water of depth H

$$G(x,0;\xi,0) = \sin|\xi - x| - \frac{1}{\pi}g(|\xi - x|) \approx A_0 \sin|\xi - x| - \sum_{n=1}^{\infty} A_n \mathrm{e}^{-\mathrm{i}\sigma_n|\xi - x|}, \tag{44}$$

where $A_0 = \frac{1}{\omega^2 + H(1-\omega^4)}$, $A_n = \frac{\mathrm{i}\sigma_n}{\omega^2 + H(\sigma_n^2 - \omega^4)}$ and the quantities σ_n are the (nondimensional) roots of the dispersion equation $\sigma\tanh\sigma H = \omega^2$ on the negative imaginary axis. By differentiating this series approximation for $g(x)$, we can derive a series approximation for $f(x)$, i.e.,

$$f(x) \approx \begin{cases} \sum\limits_{n=1}^{\infty} B_n \mathrm{e}^{\beta_n x}, & x < 0, \quad \text{where } B_n = \pi\left(\dfrac{1-\sigma_n^2}{\mathrm{i}\sigma_n}\right)A_n,\ \beta_n = 1 + \mathrm{i}\sigma_n, \\ 0, & x > 0. \end{cases} \tag{45}$$

Taking the Fourier transform of (45), we get a series approximation for $\hat{f}(k)$, as follows:

$$\hat{f}(k) \approx \sum_{n=1}^{\infty} \frac{B_n}{\beta_n + \mathrm{i}k}. \tag{46}$$

Substitution in (43) then gives a series approximation for $q(x,z)$

$$q(x,z) \approx \sum_{n=1}^{\infty} \frac{B_n}{2\pi\mathrm{i}} \int_{-\infty}^{\infty} f_n(k,x,z)\mathrm{d}k, \tag{47}$$

where $f_n(k,x,z) = \frac{-\mathrm{i}\chi(k,z)\mathrm{e}^{-\mathrm{i}kx}}{(\beta_n + \mathrm{i}k)(k\tanh kH - 4\omega^2)}$.

By shifting the poles of $(k\tanh kH - 4\omega^2)$ slightly off the real axis and evaluating the integrals around a contour in the upper half-plane for $x > 0$ and in the lower half-plane for $x < 0$, we can then use the residue theorem to obtain

$$q(x,z) \approx \Re\mathfrak{e}\begin{cases} \sum\limits_{n=1}^{\infty} B_n \left\{\mathrm{Res}[f_n, \mathrm{i}\beta_n] + \mathrm{Res}_{\epsilon\to 0}[f_n, \sigma_0^{(2)} + \mathrm{i}\epsilon] + \sum\limits_{m=1}^{\infty}\mathrm{Res}[f_n, -\sigma_m^{(2)}]\right\}, & x < 0, \\ -\sum\limits_{n=1}^{\infty} B_n \left\{\mathrm{Res}_{\epsilon\to 0}[f_n, -\sigma_0^{(2)} - \mathrm{i}\epsilon] + \sum\limits_{m=1}^{\infty}\mathrm{Res}[f_n, \sigma_m^{(2)}]\right\}, & x > 0. \end{cases} \tag{48}$$

Note we have taken the real part to eliminate the imaginary asymptotic terms that arise from the residues $\mathrm{Res}_{\epsilon\to 0}[f_n, -\sigma_0^{(2)} - \mathrm{i}\epsilon]$ and $\mathrm{Res}_{\epsilon\to 0}[f_n, \sigma_0^{(2)} + \mathrm{i}\epsilon]$ in a similar manner to those in the finite depth Green's function. Thus we get

$$q(x,z) \approx \mathfrak{Re}\left\{\begin{array}{ll} \displaystyle\sum_{n=1}^{\infty} B_n \left\{ \frac{-\chi(\mathrm{i}\beta_n, z)\mathrm{e}^{\beta_n x}}{(\mathrm{i}\beta_n \tanh(\mathrm{i}\beta_n H) - 4\omega^2)} + \frac{\mathrm{i}\sigma_0^{(2)}\chi(-\sigma_0^{(2)}, z)\mathrm{e}^{\mathrm{i}\sigma_0^{(2)}x}}{(\beta_n - \mathrm{i}\sigma_0^{(2)})(4\omega^2 + H\left((\sigma_0^{(2)})^2 - 16\omega^4\right))} \right. & \\ \qquad \left. - \displaystyle\sum_{m=1}^{\infty} \frac{\mathrm{i}\chi(\sigma_m^{(2)}, z)\mathrm{e}^{-\mathrm{i}\sigma_m^{(2)}x}}{(\beta_n + \mathrm{i}\sigma_m^{(2)})\left(4\omega^2 + H\left((\sigma_m^{(2)})^2 - 16\omega^4\right)\right)} \right\}, & x < 0, \\ -\displaystyle\sum_{n=1}^{\infty} B_n \left\{ \frac{\mathrm{i}\sigma_0^{(2)}\chi(-\sigma_0^{(2)}, z)\mathrm{e}^{\mathrm{i}\sigma_0^{(2)}x}}{(\beta_n - \mathrm{i}\sigma_0^{(2)})\left(4\omega^2 + H\left((\sigma_0^{(2)})^2 - 16\omega^4\right)\right)} \right. & \\ \qquad \left. - \displaystyle\sum_{m=1}^{\infty} \frac{\mathrm{i}\sigma_m^{(2)}\chi(\sigma_m^{(2)}, z)\mathrm{e}^{-\mathrm{i}\sigma_m^{(2)}x}}{(\beta_n + \mathrm{i}\sigma_m^{(2)})\left(4\omega^2 + H\left((\sigma_m^{(2)})^2 - 16\omega^4\right)\right)} \right\}, & x > 0, \end{array}\right. \tag{49}$$

which is shown in Fig. 3.

To give us confidence, we may reconcile the asymptotic behaviour of this approximation with that of the corresponding infinite depth wave-type singular potential in (78), i.e.,

$$\begin{aligned} \lim_{x\to\pm\infty} q(x,z) &= \mp\mathfrak{Re}\left\{\left(\hat{f}_1(\sigma_0^{(2)}) + \mathrm{i}\hat{f}_2(\sigma_0^{(2)})\right)\mathrm{e}^{\pm\mathrm{i}\sigma_0^{(2)}x}\right\} \times \frac{\sigma_0^{(2)}\chi(\sigma_0^{(2)}, z)}{4\omega^2 + H\left((\sigma_0^{(2)})^2 - 16\omega^4\right)} \\ &\to \mp\left(\hat{f}_1(4)\cos 4x - \hat{f}_2(4)\sin 4x\right)\mathrm{e}^{-4z}, \quad \text{as } H\to\infty, \end{aligned} \tag{50}$$

i.e., this is consistent with the asymptotic limit of the infinite depth wave-type singular potential given in (78).

Finally, it is relevant to consider whether the finite-depth wave-type singular potential calculated above using residues could also be found using the so called matching method (see, e.g. [18]). We propose the solution

$$q(x,z) = \breve{q}(x,z) + \hat{q}(x,z), \tag{51}$$

where $\breve{q}(x,z)$, the homogeneous part of the solution, is given by

$$\breve{q}(x,z) = \begin{cases} -\breve{b}_0\mathrm{e}^{-\mathrm{i}\sigma_0^{(2)}x}\chi(\sigma_0^{(2)}, z) + \displaystyle\sum_{n=0}^{\infty}\breve{a}_n\mathrm{e}^{\mathrm{i}\sigma_n^{(2)}x}\chi(\sigma_n^{(2)}, z), & x < 0, \\ -\breve{a}_0\mathrm{e}^{\mathrm{i}\sigma_0^{(2)}x}\chi(\sigma_0^{(2)}, z) + \displaystyle\sum_{n=0}^{\infty}\breve{b}_n\mathrm{e}^{-\mathrm{i}\sigma_n^{(2)}x}\chi(\sigma_n^{(2)}, z), & x > 0, \end{cases} \tag{52}$$

and

$$\hat{q}(x,z) = \begin{cases} \displaystyle\sum_{n=1}^{\infty}\hat{a}_n\mathrm{e}^{\beta_n x}\chi(\mathrm{i}\beta_n, z), \quad \hat{a}_n = \frac{-B_n}{\mathrm{i}\beta_n\tanh(\mathrm{i}\beta_n H) - 4\omega^2}, & x < 0, \\ 0, & x > 0. \end{cases} \tag{53}$$

Then we should be able to use the continuity conditions

$$q(0^-, z) = q(0^+, z), \quad q_x(0^-, z) = q_x(0^+, z), \tag{54a,b}$$

to get the equations

$$\int_0^H \left(\breve{q}(0^-, z) - \breve{q}(0^+, z)\right)\chi(\sigma_m^{(2)}, z)\mathrm{d}z = -\int_0^H \hat{q}(0^-, z)\chi(\sigma_m^{(2)}, z)\mathrm{d}z, \quad m = 0, 1, 2, \ldots \tag{55a}$$

$$\int_0^H \left(\breve{q}_x(0^-, z) - \breve{q}_x(0^+, z)\right)\chi(\sigma_m^{(2)}, z)\mathrm{d}z = -\int_0^H \hat{q}_x(0^-, z)\chi(\sigma_m^{(2)}, z)\mathrm{d}z, \quad m = 0, 1, 2, \ldots \tag{55b}$$

These equations can actually be solved separately for each pair of unknown coefficients $\breve{a}_m, \breve{b}_m$. We can obviously use the equations to approximate the solution by truncating the series on the LHS at $n = N_2$ and on the RHS at $n = N_1$. In Fig. 4 we use this method to approximate $q(x, 0)$ with $H = 200$ m.

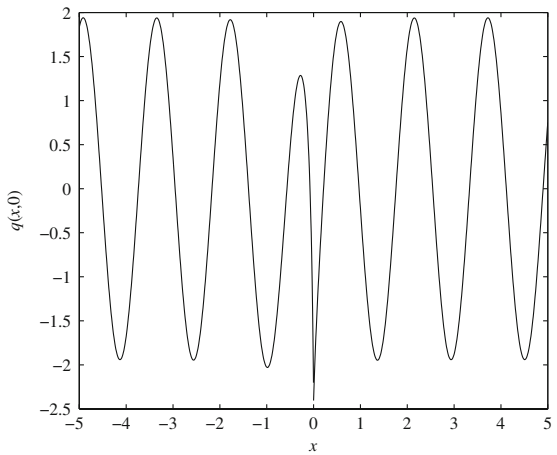

Fig. 3 The residue solution for $q(x, 0)$ in depth $H = 200$ m, cf. Fig. 8

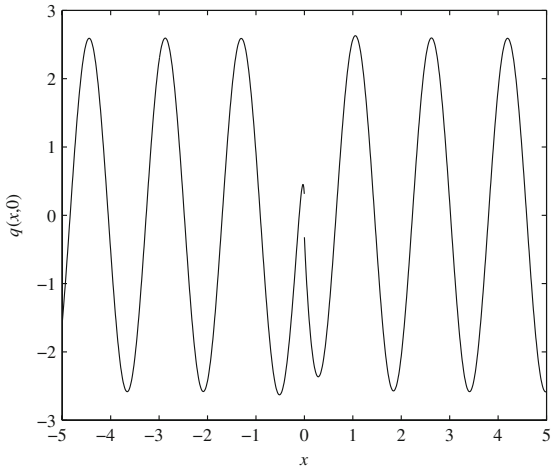

Fig. 4 The matching solution for $q(x, 0)$ in depth $H = 200$ m, with $N_1 = N_2 = 100$

Table 1 Convergence of matching solution, for $H = 200$ m

N_1	$-\int_0^H \hat{q}(0^-, z)\chi(\sigma_0^{(2)}, z)\mathrm{d}z$	$-\int_0^H \hat{q}_x(0^-, z)\chi(\sigma_0^{(2)}, z)\mathrm{d}z$
100	0.2428	1.0275
500	0.3114	2.4954
1,000	0.3213	3.1756
2,000	0.3264	3.8628

It is evident, however, that this approximation disagrees markedly from the solution plotted in Fig. 3 (and in Fig. 8 for infinite depth). Moreover, this solution is highly unstable as one varies N_1 and N_2 and it appears that the matching approximation is at fault. We can unearth the principal source of this error by considering the equations for $\check{a}_0, \check{b}_0$ $(m = 0)$, which determine the asymptotic behaviour of the solution. From the residue solution derived earlier we can actually see what the RHS of the equation should approximate, i.e.,

$$2(\check{a}_0 - \check{b}_0)K_0 = -\sum_{n=1}^{\infty} \hat{a}_n \int_0^H \chi(\mathrm{i}\beta_n, z)\chi(\sigma_0^{(2)}, z)\mathrm{d}z \approx \frac{\arctan \sigma_0^{(2)}}{\sigma_0^{(2)}}, \tag{56a}$$

$$2\mathrm{i}\sigma_0^{(2)}(\check{a}_0 + \check{b}_0)K_0 = -\sum_{n=1}^{\infty} \beta_n \hat{a}_n \int_0^H \chi(\mathrm{i}\beta_n, z)\chi(\sigma_0^{(2)}, z)\mathrm{d}z \approx -\frac{1}{2}\log[1 + (\sigma_0^{(2)})^2], \tag{56b}$$

where $K_0 = \int_0^H \chi(\sigma_0^{(2)}, z)^2\mathrm{d}z$. The asymptotic behaviour of the solutions plotted in Figs. 3, 4 differ because the matching approximations are poor, even when N_1 is very large, as indicated in the Table 1. While the first column in the table (slowly) converges to $\arctan \sigma_0^{(2)}/\sigma_0^{(2)} = 0.3315$, as it should according to (56a), the second column is obviously not converging to the RHS of (56b), i.e., to $-\log[1 + (\sigma_0^{(2)})^2]/2 = -1.4166$.

7 Results and conclusions

The principal goal of this paper has been to present a second-order theory that describes how a flexible (hydroelastic) raft is affected by a large-amplitude ocean-wave train. To allow for some generality, the raft has been represented mathematically using three different nonlinear mechanical models, due to Forbes [25,26], von Kármán

[27, Sect. 16.9], [28, Sect. 8.5] and Drozdov [29, pp. 191–196]. In doing this we have also shown that the second-order eigenfunction matching theory of [16], which was originally constructed to model a semi-infinite flexible sea-ice cover subjected to waves, produces unacceptably inaccurate results when it is applied to a finite raft in water of finite depth.

To conclude, we present some results using, by way of example, physical material parameters that are typical of sea-ice, namely, $E = 5\,\mathrm{GPa}$, $\nu = 0.3$, $\rho_i = 922.5\,\mathrm{kg\,m^{-3}}$, $\rho_w = 1{,}025\,\mathrm{kg\,m^{-3}}$. The purpose of these plots is not intended to be geophysical; rather the curves are plotted to allow the magnitude of the first- and second-order solutions to be directly compared to determine when a linear theory will suffice and when it is necessary to use a higher-order theory. Similar calculations can be done for a pontoon-type hydroelastic VLFS or a flexible breakwater, although by chance it turns out that in practice sea-ice physical constants are quite close to those for other floating bodies of this type. The von Kármán plate [27, Sect. 16.9], [28, Sect. 8.5] is used again here but recall the other two models actually produce very similar results.

Figures 5–7 show these comparisons for a 50 m ice floe in waves of (normalized) amplitude $a = 1\,\mathrm{m}$ at 5 s, 10 s and 20 s period, respectively. Evidently the wave period and the wave amplitude are pivotal in determining the importance of higher-order effects: essentially the smaller the period or the larger the amplitude the greater is the relative importance of the second-order terms in comparison with the first-order ones. This, of course, is not an unexpected result but reassuringly the study has confirmed and quantified our intuition for the specific case of a floating hydroelastic raft. By way of example, the second-order contribution in (12b) for a 5-s-period, 1-m-amplitude wave is more than 50% of the magnitude of the first-order term, while at 10 s the ratio has dropped to less than 10% and at 20 s it is only a few percent.

Recalling our comments about global warming at the beginning of the paper and the associated proliferation of intense storms with their simultaneous severe waves, it is important to remind the reader that the ratio of second-order to first-order effects is proportional to wave amplitude (12b). Accordingly, putting aside any change to the spectral composition of the oceans and marginal seas in the future, as it is difficult to anticipate what will actually occur, it still remains highly probable that nonlinear effects will become far more prevalent. Storms of much greater destructive power will drive their waves further into ice fields, causing major challenges for existing and proposed oil

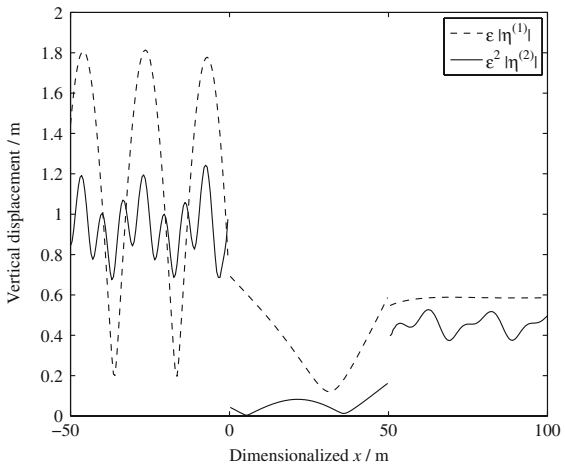

Fig. 5 Absolute values of vertical displacements $\epsilon|\eta^{(1)}|$ and $\epsilon^2|\eta^{(2)}|$, where $\epsilon = a\omega^2/g$, when $a = 1\,\mathrm{m}$, $T = 5\,\mathrm{s}$ and $L = 50\,\mathrm{m}$. The figure shows the displacement in the open water on either side of the ice floe, stretching from $-50\,\mathrm{m}$ to 0 m and from 50 m to 100 m, and the deflection of the floe from 0 to 50 m. First-order displacement is shown dashed and second-order displacement is shown solid

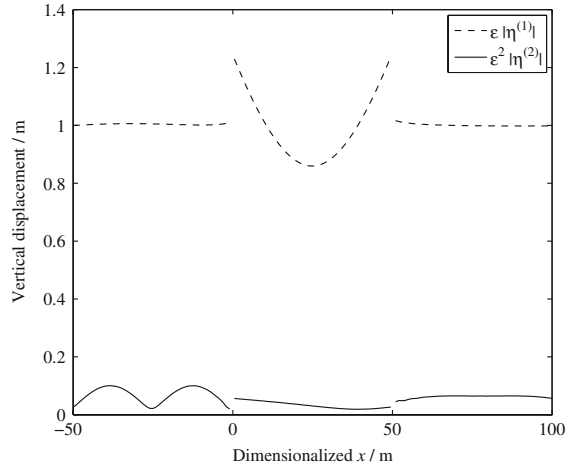

Fig. 6 As Fig. 5 but for $T = 10\,\mathrm{s}$

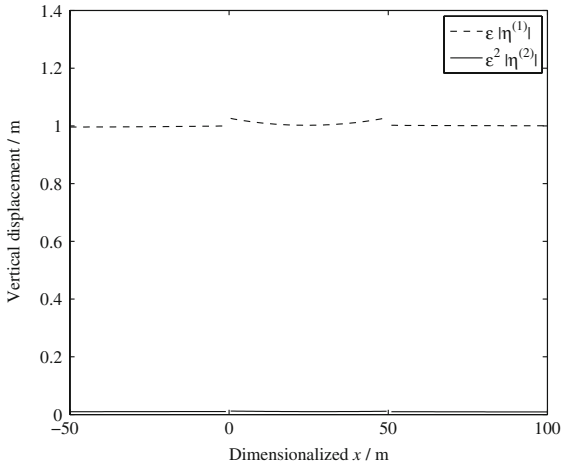

Fig. 7 As Fig. 5 but for $T = 20\,\mathrm{s}$

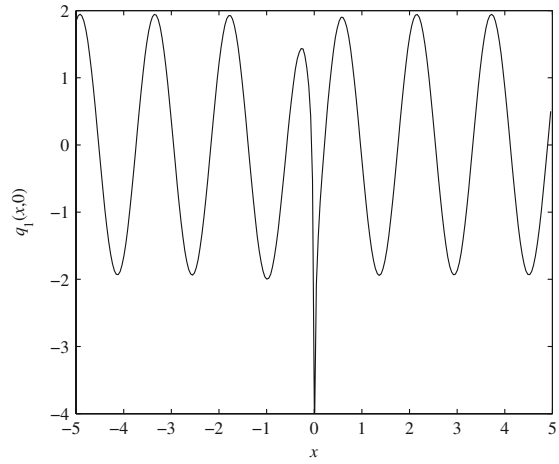

Fig. 8 Approximation of $q_1(x, 0)$ plotted against the nondimensional coordinate x for water of infinite depth

and gas installations, and in ice-free regions offshore structures and seagoing vessels will be subjected to amplified wave-induced flexure and potential damage.

Acknowledgements Supported by the Marsden Fund Council from Government funding administered by the Royal Society of New Zealand, and by the University of Otago. The authors also wish to thank colleagues Dr Tony Dixon, whose work provided much of the background for this paper, and Dr Tim Williams for several key insights.

Appendix A: Singular expansion

In the following it is important to be able to compute the first and second derivatives of $\phi^{(1)}(x, 0)$ accurately. However, one cannot simply differentiate (30a) with respect to x since $\tilde{G}_x$ has a $1/x$ type singularity at $\xi = x$, so our formula for $\phi_x^{(1)}$ would have logarithmic-type singularities at each node. To sidestep this problem and to assist in the integration of these functions in Sect. 5 we extract their singular components, i.e.,

$$\phi_x^{(1)} = \hat{\phi}_x^{(1)} + a_1 \log|x| + a_2 \log|L - x|, \tag{57}$$

where $a_1 = \psi(0^+)/\pi$, $a_2 = \psi(L^-)/\pi$ and the nonsingular part $\hat{\phi}_x^{(1)}$ is given by

$$\hat{\phi}_x^{(1)} = \begin{cases} -\mathrm{i}e^{-\mathrm{i}x} - (a_1 + a_2)\log|L - x| + \displaystyle\int_0^L \left[\tilde{G} - \frac{1}{\pi}\log|\xi - x|\right]_x \psi(\xi)\mathrm{d}\xi \\ \quad - \dfrac{1}{\pi}\displaystyle\int_0^L \frac{\psi(0^+) - \psi(\xi)}{x - \xi}\mathrm{d}\xi, & x < 0, \\ -\mathrm{i}e^{-\mathrm{i}x} - \dfrac{1}{\pi}\big(\psi(0^+) - \psi(x)\big)\log|x| + \dfrac{1}{\pi}\big(\psi(L^-) - \psi(x)\big)\log|L - x| \\ \quad + \displaystyle\int_0^L \left[\tilde{G} - \frac{1}{\pi}\log|\xi - x|\right]_x \psi(\xi)\mathrm{d}\xi - \dfrac{1}{\pi}\displaystyle\int_0^L \frac{\psi(x) - \psi(\xi)}{x - \xi}\mathrm{d}\xi, & 0 < x < L, \\ -\mathrm{i}e^{-\mathrm{i}x} - (a_1 + a_2)\log|x| + \displaystyle\int_0^L \left[\tilde{G} - \frac{1}{\pi}\log|\xi - x|\right]_x \psi(\xi)\mathrm{d}\xi \\ \quad - \dfrac{1}{\pi}\displaystyle\int_0^L \frac{\psi(L^-) - \psi(\xi)}{x - \xi}\mathrm{d}\xi, & x > L. \end{cases} \tag{58}$$

Using this expression, we may then expand the second derivative as

$$\phi^{(1)}_{xx} = \hat{\phi}^{(1)}_{xx} + b_1 \log|x| + b_2 \log^2|x| + \frac{b_3}{x} + b_4 \log|L-x| + b_5 \log^2|L-x| + \frac{b_6}{x-L}, \tag{59}$$

where the constants $b_1, \ldots, b_6$ are given by

$$b_1 = (h(0) + a_2 \log L)/\pi, \quad b_2 = a_1/2\pi, \quad b_3 = a_1,$$
$$b_4 = -(h(L) + a_1 \log L)/\pi, \quad b_5 = -a_2/2\pi, \quad b_6 = a_2,$$

and $h(x) = \hat{\phi}^{(1)}_x + \phi^{(1)}_{n_x}(x,0)$, $0 \le x \le L$.

The nonsingular part $\hat{\phi}^{(1)}_{xx}$ is given by

$$\hat{\phi}^{(1)}_{xx} = \begin{cases} -\mathrm{e}^{-\mathrm{i}x} + (h(L)-h(0))\log|L-x|/\pi + \dfrac{a_1}{\pi}\left(\pi^2/6 + \log^2(L)/2 + \mathrm{Li}_2(x/L)\right) \\ \quad + \dfrac{a_2}{\pi}\left(\pi^2/3 - \mathfrak{Re}[\mathrm{Li}_2(1-x/L)] - \log^2(L)/2\right) + \displaystyle\int_0^L \left[\tilde{G} - \frac{1}{\pi}\log|\xi - x|\right]_{xx} \psi(\xi)\mathrm{d}\xi \\ \quad - \dfrac{1}{\pi}\displaystyle\int_0^L \frac{h(0)-h(\xi)}{x-\xi}\mathrm{d}\xi, & x < 0, \\ -\mathrm{e}^{-\mathrm{i}x} + \psi(x) - (h(0)-h(x))\log|x|/\pi + (h(L)-h(x))\log|L-x|/\pi \\ \quad - \dfrac{a_1}{\pi}\left(\pi^2/3 - \log^2(L)/2 - \mathrm{Li}_2(x/L)\right) + \dfrac{a_2}{\pi}\left(\pi^2/3 - \log^2(L)/2 - \mathrm{Li}_2(1-x/L)\right) \\ \quad - \displaystyle\int_0^L \tilde{G}(\xi,x)\psi(\xi)\mathrm{d}\xi - \frac{1}{\pi}\int_0^L \frac{h(x)-h(\xi)}{x-\xi}\mathrm{d}\xi, & 0<x<L, \\ -\mathrm{e}^{-\mathrm{i}x} + (h(L)-h(0))\log|x|/\pi - \dfrac{a_2}{\pi}\left(\pi^2/6 + \log^2(L)/2 + \mathrm{Li}_2(1-x/L)\right) \\ \quad - \dfrac{a_1}{\pi}\left(\pi^2/3 - \mathfrak{Re}[\mathrm{Li}_2(x/L)] - \log^2(L)/2\right) + \displaystyle\int_0^L \left[\tilde{G} - \frac{1}{\pi}\log|\xi - x|\right]_{xx} \psi(\xi)\mathrm{d}\xi \\ \quad - \dfrac{1}{\pi}\displaystyle\int_0^L \frac{h(L)-h(\xi)}{x-\xi}\mathrm{d}\xi, & x > L, \end{cases} \tag{60}$$

where Li_2 is the dilogarithm (defined in [32, Sect. 27.7] or, equivalently, in [33, p. 435]).

These expansions of $\phi^{(1)}_x$ and $\phi^{(1)}_{xx}$ then allow us to expand a function that is important in the second-order analysis similarly, namely

$$K(x) = B(x) - 2\mathrm{i}A(x) = \left(\eta^{(1)}_x \phi^{(1)}_x - \eta^{(1)}\phi^{(1)}_{zz}\right) - \mathrm{i}\left((\phi^{(1)}_x)^2 + (\phi^{(1)}_z)^2 - 2\mathrm{i}\eta^{(1)}\phi^{(1)}_z\right), \tag{61}$$

evaluated on the surface. This simplifies to

$$K(x) = \begin{cases} \mathrm{i}\phi^{(1)}_x \phi^{(1)}_{zx} + \mathrm{i}\phi^{(1)}_z \phi^{(1)}_{xx} - \mathrm{i}(\phi^{(1)}_x)^2 - 3\mathrm{i}(\phi^{(1)}_z)^2, & 0 < x < L, \\ -2\mathrm{i}(\phi^{(1)}_x)^2 - \mathrm{i}\phi^{(1)}\phi^{(1)}_{xx} - 3\mathrm{i}(\phi^{(1)})^2, & \text{otherwise.} \end{cases} \tag{62}$$

An important property of this function can be established by substituting the asymptotic limits of $\phi^{(1)}$ and its derivatives in the second of these two formulae, namely $K(x) \to -8\mathrm{i}R^{(1)}$ as $x \to -\infty$ and $K(x) \to 0$ as $x \to +\infty$.

The expansions of $\phi^{(1)}_x$ and $\phi^{(1)}_{xx}$ above allow us to expand $K(x)$ in a similar way, i.e., $K(x) = K_1(x) + K_2(x)$, where K_2 shares the asymptotic properties of K and has integrable log and $\log^2$ singularities at 0 and L, while the non-integrable part is of the form

$$K_1(x) = c_1 \frac{\mathrm{e}^x U(-x)}{x} + c_2 \frac{\mathrm{e}^{-x} U(x)}{-x} + c_3 \frac{\mathrm{e}^{x-L} U(L-x)}{x-L} + c_4 \frac{\mathrm{e}^{L-x} U(x-L)}{L-x}, \tag{63}$$

where $c_1 = -\mathrm{i}a_1\phi^{(1)}(0,0)$, $c_2 = -\mathrm{i}a_1\phi^{(1)}_z(0^+,0)$, $c_3 = \mathrm{i}a_2\phi^{(1)}_z(L^-,0)$, $c_4 = \mathrm{i}a_2\phi^{(1)}(L,0)$ and $U(x)$ is the unit step (Heaviside) function. The reason for this decomposition will become clear in the second-order solution.

Appendix B: Singular potentials

B.1 Neumann-type singular potential

Here we wish to find the solution $q(x, z)$ of the Neumann problem

$$\Delta q = 0, \quad z > 0, \tag{64a}$$

$$q_z(x, 0) = f(x), \quad z = 0, \tag{64b}$$

$$q_z \to 0, \quad z \to \infty, \tag{64c}$$

This problem is solved by means of Fourier transforms, i.e.,

$$q(x, z) = -\frac{1}{2\pi} \int_{-\infty}^{\infty} \frac{\hat{f}(k)}{|k|} \mathrm{e}^{-\mathrm{i}kx - |k|z} \mathrm{d}k. \tag{65}$$

We denote this integral for $f(x) = \mathrm{e}^x U(-x)/x$, where $U(x)$ is the unit step (Heaviside) function, by $q_1(x, z)$ and note that for $z = 0$ this is given by $q_1(x, 0) = -\mathcal{F}^{-1}(\hat{f}(k)/|k|)$.

The Fourier transform of $f(x) = \mathrm{e}^x U(-x)/x$ is given by

$$\hat{f}(k) = \mathrm{i}\hat{f}_1(k) + \hat{f}_2(k) = \mathrm{i}\arctan(k) + \frac{1}{2}\log(1 + k^2). \tag{66}$$

To find $q_1(x, 0)$ we first consider the first part, namely

$$\mathcal{F}^{-1}\left\{\frac{\arctan(k)}{|k|}\right\} = \mathcal{F}^{-1}\left\{\frac{\arctan(k)}{|k|} - \mathrm{sgn}(k)\mathrm{e}^{-|k|} - \frac{\pi k}{2(k^2+1)}\right\} - \frac{\mathrm{i}x}{\pi(x^2+1)} - \frac{\mathrm{i}\pi}{4}\mathrm{sgn}(x)\mathrm{e}^{-|x|}, \tag{67}$$

where the inverse transform on the RHS of this expression is approximated using FFT. The other part of $q_1(x, 0)$ requires the inverse transform

$$\mathcal{F}^{-1}\left\{\frac{\log(1+k^2)}{2|k|}\right\} = \mathcal{F}^{-1}\left\{\frac{\log(1+k^2)}{2|k|} - \frac{|k|\log|k|}{1+k^2}\right\} + \mathcal{F}^{-1}\left\{\frac{|k|\log|k|}{1+k^2}\right\}, \tag{68}$$

partitioned such that the first term on the RHS can again be approximated by FFT, while the second part is expressed as the convolution

$$\mathcal{F}^{-1}\left\{\frac{|k|\log|k|}{1+k^2}\right\} = \mathcal{F}^{-1}\{\mathrm{sgn}(k)\log|k|\} * \mathcal{F}^{-1}\left\{\frac{k}{k^2+1}\right\} = \frac{1}{2\pi}\,\mathrm{p.v.}\int_{-\infty}^{\infty} \frac{\gamma + \log|x-\xi|}{x-\xi}\mathrm{sgn}(\xi)\mathrm{e}^{-|\xi|}\mathrm{d}\xi. \tag{69}$$

This may be simplified using integration by parts, as follows:

$$\mathrm{p.v.}\int_{-\infty}^{\infty} \frac{\gamma + \log|x-\xi|}{x-\xi}\,\mathrm{sgn}(\xi)\mathrm{e}^{-|\xi|}\mathrm{d}\xi = \log^2|x| + 2\gamma\log|x| - \frac{1}{2}\int_{-\infty}^{\infty}\left(\log^2|x-\xi| + 2\gamma\log|x-\xi|\right)\mathrm{e}^{-|\xi|}\mathrm{d}\xi, \tag{70}$$

and the remaining integrals can be written in terms of special functions, i.e.,

$$\begin{aligned}\int_{-\infty}^{\infty} \log^2|x-\xi|\,\mathrm{e}^{-|\xi|}\mathrm{d}\xi = \mathrm{e}^{-|x|}&\left(\gamma^2 + \frac{\pi^2}{6} + 2|x|{}_3F_3(1,1,1;2,2,2;|x|)\right.\\ &\left. + \log|x|\left[2\gamma - 2E_1(|x|)(1+\mathrm{e}^{|x|})\log|x|\right]\right)\\ +\mathrm{e}^{|x|}&\left(\gamma^2 + \frac{\pi^2}{6} - 2|x|{}_3F_3(1,1,1;2,2,2;-|x|)\right.\\ &\left. + \log|x|\left[2\gamma + 2E_1(|x|) + (1+\mathrm{e}^{-|x|})\log|x|\right]\right),\end{aligned} \tag{71}$$

and

$$\int_{-\infty}^{\infty} \log|x-\xi|\,\mathrm{e}^{-|\xi|}\mathrm{d}\xi = 2\log|x| + \mathrm{e}^{|x|}E_1(|x|) - \mathrm{e}^{-|x|}E_1(|x|), \tag{72}$$

where $E_1(\cdot)$ denotes the exponential integral, in this case for positive real argument, and ${}_3F_3(\cdot)$ is a generalized hypergeometric function [33, pp. 724–725] (see also [32, Chapt. 15]).

Thus, collecting the details of (67)–(72), we have

$$\begin{aligned} q_1(x,0) = -\mathrm{i}\mathcal{F}^{-1}\left\{\frac{\arctan(k)}{|k|} - \operatorname{sgn}(k)\mathrm{e}^{-|k|} - \frac{\pi k}{2(k^2+1)}\right\} - \mathcal{F}^{-1}\left\{\frac{\log(1+k^2)}{2|k|} - \frac{|k|\log|k|}{1+k^2}\right\} - \frac{x}{\pi(x^2+1)} \\ -\frac{\pi}{4}\operatorname{sgn}(x)\mathrm{e}^{-|x|} - \frac{1}{2\pi}\log^2|x| - \frac{\gamma}{\pi}\log|x| + \mathrm{e}^{-|x|}\left(\gamma^2 + \frac{\pi^2}{6} + 2|x|{}_3F_3(1,1,1;2,2,2;|x|)\right. \\ \left. + \frac{\log|x|}{4\pi}\left[2\gamma - 2E_1(|x|) + (1+\mathrm{e}^{|x|})\log|x|\right]\right) + \frac{\mathrm{e}^{|x|}}{4\pi}\left(\gamma^2 + \frac{\pi^2}{6} - 2|x|{}_3F_3(1,1,1;2,2,2;-|x|)\right. \\ \left. + \log|x|\left[2\gamma + 2E_1(|x|) + (1+\mathrm{e}^{-|x|})\log|x|\right]\right) + \frac{\gamma}{2\pi}\left(2\log|x| + \mathrm{e}^{|x|}E_1(|x|) - \mathrm{e}^{-|x|}E_1(|x|)\right). \end{aligned} \tag{73}$$

Finally we consider the integral (65) for $f(x) = K_1(x)$. Since $K_1(x)$ is made up of four similar components in (63), the other components of q are defined by symmetry and translation, i.e., if $\partial q_2/\partial z = -\mathrm{e}^{-x}U(x)/x$ then $q_2(x,z) = q_1(-x,z)$ and similarly $q_3(x,z) = q_1(x-L,z)$, $q_4(x,z) = q_2(x-L,z)$. Finally $q(x,z)$ is assembled

$$q(x,z) = c_1q_1(x,z) + c_2q_2(x,z) + c_3q_3(x,z) + c_4q_4(x,z). \tag{74}$$

B.2 Wave-type singular potential

Another way to deal with the singular boundary terms is to use the solution of

$$\Delta q = 0, \quad z > 0, \tag{75a}$$

$$q_z + 4q = f(x), \quad z = 0, \tag{75b}$$

$$q_z \to 0, \quad z \to \infty, \tag{75c}$$

which can clearly be expressed in terms of the integral

$$q(x,z) = -\frac{1}{2\pi}\int_{-\infty}^{\infty}\frac{\hat{f}(k)}{|k|-4}\mathrm{e}^{-\mathrm{i}kx-|k|z}\mathrm{d}k. \tag{76}$$

We denote this integral for $f(x) = \mathrm{e}^xU(-x)/x$ by $q_1(x,z)$ and approximate it at $z = 0$ as

$$\begin{aligned} q_1(x,0) = -\mathrm{i}\mathcal{F}^{-1}\left\{\frac{\arctan(k)}{|k|-4} - \frac{\arctan(4)}{k-4} - \frac{\arctan(4)}{k+4} - \frac{\pi k(1-2\arctan(4))}{2(k^2+1)}\right\} \\ -\mathcal{F}^{-1}\left\{\frac{\log(1+k^2)}{2(|k|-4)} - \frac{\log\sqrt{17}}{k-4} + \frac{\log\sqrt{17}}{k+4} - \frac{|k|\log|k|}{1+k^2}\right\} + \frac{\mathrm{ie}^{-4\mathrm{i}x}}{2}(\mathrm{i}\arctan(4) + \log\sqrt{17})\operatorname{sgn}(x) \\ + \frac{\mathrm{ie}^{4\mathrm{i}x}}{2}(\mathrm{i}\arctan(4) - \log\sqrt{17})\operatorname{sgn}(x) - \frac{\pi\mathrm{e}^{-|x|}}{4}(1-2\arctan(4))\operatorname{sgn}(x) - \mathcal{F}^{-1}\left\{\frac{|k|\log|k|}{k^2+1}\right\}, \end{aligned} \tag{77}$$

where the first two terms are found using FFT and the rest are evaluated exactly. This is plotted in Fig. 8, where in this and subsequent plots the von Kármán plate has been used, although in fact the difference between models is minimal. As before, the other components of $q(x,z)$ for $f(x) = K_1(x)$ may be defined by symmetry and translation, and assembled as in (74).

Note that we do not have to be very careful in approximating this function, as it will turn out that we only need $q(x,0)$ for $0 < x < L$ in the boundary-integral method. We can also use the integral formula to derive the asymptotic behaviour of $q(x,z)$, i.e., letting $f(x) = K_1(x)$ assembled according to (63), we obtain

$$\lim_{x\to\pm\infty} q(x,z) = \pm\left(\frac{\alpha_1}{2}\mathrm{e}^{4\mathrm{i}x} + \frac{\alpha_2}{2}\mathrm{e}^{-4\mathrm{i}x}\right)\mathrm{e}^{-4z}, \tag{78}$$

where

$$\alpha_1 = -c_1\left(\hat{f}_1(4)+\mathrm{i}\hat{f}_2(4)\right)+c_2\left(\hat{f}_1(4)-\mathrm{i}\hat{f}_2(4)\right)-c_3\mathrm{e}^{-4\mathrm{i}L}\left(\hat{f}_1(4)+\mathrm{i}\hat{f}_2(4)\right)+c_4\mathrm{e}^{-4\mathrm{i}L}\left(\hat{f}_1(4)-\mathrm{i}\hat{f}_2(4)\right), \tag{79}$$

$$\alpha_2 = -c_1\left(\hat{f}_1(4)-\mathrm{i}\hat{f}_2(4)\right)+c_2\left(\hat{f}_1(4)+\mathrm{i}\hat{f}_2(4)\right)-c_3\mathrm{e}^{4\mathrm{i}L}\left(\hat{f}_1(4)-\mathrm{i}\hat{f}_2(4)\right)+c_4\mathrm{e}^{4\mathrm{i}L}\left(\hat{f}_1(4)+\mathrm{i}\hat{f}_2(4)\right). \tag{80}$$

and $\hat{f}_1$, $\hat{f}_2$ are given in (66).

References

1. Squire VA (2007) Of ocean waves and sea-ice revisited. Cold Reg Sci Technol 49(2):110–133
2. Balmforth NJ, Craster RV (1999) Ocean waves and ice sheets. J Fluid Mech 395:89–124
3. Chakrabarti A (2000) On the solution of the problem of scattering of surface-water waves by the edge of an ice cover. Proc R Soc Lon Ser-A 456(1997):1087–1099
4. Squire VA, Dixon TW (2000) An analytic model for wave propagation across a crack in an ice sheet. Int J Offshore Polar 10(3):173–176
5. Squire VA, Dixon TW (2001) How a region of cracked sea ice affects ice-coupled wave propagation. Ann Glaciol 33:327–332
6. Squire VA, Dixon TW (2001) On modelling an iceberg embedded in shore fast sea ice. J Eng Math 40(3):211–236
7. Sahoo T, Yip TL, Chwang AT (2001) Scattering of surface waves by a semi-infinite floating elastic plate. Phys Fluids 13(11):3215–3222
8. Linton CM, Chung H (2003) Reflection and transmission at the ocean/sea-ice boundary. Wave Motion 38(1):43–52
9. Porter D, Porter R (2004) Approximations to wave scattering by an ice sheet of variable thickness over undulating bed topography. J Fluid Mech 509:145–179
10. Chung H, Linton CM (2005) Reflection and transmission of waves across a gap between two semi-infinite elastic plates on water. Q J Mech Appl Math 58(1):1–15
11. Manam SR, Bhattacharjee J, Sahoo T (2006) Expansion formulae in wave structure interaction problems. Proc R Soc Lon Ser-A 462(2065):263–287
12. Bennetts LG, Biggs NRT, Porter D (2007) A multi-mode approximation to wave scattering by ice sheets of varying thickness. J Fluid Mech 579:413–443
13. Williams TD, Squire VA (2006) Scattering of flexural-gravity waves at the boundaries between three floating sheets with applications. J Fluid Mech 569:113–140
14. Williams TD, Squire VA (2007) Wave scattering at the sea-ice/ice-shelf transition with other applications. SIAM J Appl Math 67(4):938–959
15. Squire VA, Dugan JP, Wadhams P, Rottier PJ, Liu AK (1995) Of ocean waves and sea ice. Annu Rev Fluid Mech 27:115–168
16. Fox C (2002) Large amplitude sea/ice coupling. In: Murthy TKS, Sackinger WM, Wadhams P (eds) Advances in ice technology. Proc. 3rd Int. Conf. Ice Tech. Computational Mechanics Publications, Cambridge, MA, pp 291–304
17. Hegarty GM, Squire VA (2002) Large amplitude periodic waves beneath an ice sheet. In: Squire VA, Langhorne PJ (eds) Ice in the environment. Proceedings of the 16th international symposium on ice, vol 2. International Association of Hydraulic Engineering and Research, University of Otago, Dunedin, NZ, pp 310–317
18. Hegarty GM, Squire VA (2004) On modelling the interaction of large amplitude waves with a solitary floe. In: Chung JS, Izumiyama K, Sayed M, Hong SW (eds) Proceedings of the 14th international offshore and polar engineering conference, vol 1. International Society of Offshore and Polar Engineers, Cupertino, CA, pp 845–850
19. Rothrock DA, Yu Y, Maykut GA (1999) Thinning of the Arctic sea-ice cover. Geophys Res Lett 26(23):3469–3472
20. Wadhams P, Davis NR (2000) Further evidence of ice thinning in the Arctic Ocean. Geophys Res Lett 27(24):3973–3976
21. Comiso J (2002) A rapidly declining perennial sea-ice cover in the Arctic. Geophys Res Lett 29(20):1956. doi:10.1029/2002GL015650
22. Meylan MH, Squire VA (1994) The response of ice floes to ocean waves. J Geophys Res 99(C1):899–900
23. Eatock Taylor R (2007) Hydroelastic analysis of plates and some approximations. J Eng Math 58(1–4):267–278
24. Verne J (1896) The floating island. Sampson Low, Marston and Co, London
25. Forbes LK (1986) Surface waves of large amplitude beneath an elastic sheet. Part 1. High-order series solution. J Fluid Mech 169:409–428
26. Forbes LK (1986) Surface waves of large amplitude beneath an elastic sheet. Part 2. Galerkin solution. J Fluid Mech 188:491–508
27. Fung YC (1965) Foundations of solid mechanics. Prentice-Hall, Englewood Cliffs
28. Washizu K (1982) Variational methods in elasticity and plasticity. Pergamon, New York
29. Drozdov AD (1996) Finite elasticity and viscoelasticity: a course in the nonlinear mechanics of solids. World Scientific, Singapore
30. Stoker JJ (1957) Water waves the mathematical theory with applications. Interscience, New York
31. Williams TD (2005) Reflections on ice: the scattering of flexural-gravity waves by irregularities in Arctic and Antarctic ice sheets. PhD thesis, University of Otago, Dunedin, NZ
32. Abramowitz M, Stegun IA (1965) Handbook of mathematical functions. Dover Publications, New York
33. Weisstein EW (1999) CRC concise encyclopedia of mathematics. CRC Press, Boca Raton